# Integrated multiphysics and computational fluid dynamics modeling of a carbothermic aluminium reactor

**Light Metals 2004** *Edited by Alton T. Tabereaux* ***TMS (The Minerals, Metals & Materials Society), 2004***

# INTEGRATED MULTIPHYSICS AND COMPUTATIONAL FLUID DYNAMICS MODELING OF A CARBOTHERMIC ALUMINIUM REACTOR

Dimitrios I. Gerogiorgis and B. Erik Ydstie
Department of Chemical Engineering, Carnegie Mellon University, Pittsburgh, PA 15213, USA

## Abstract

The present simulation study elaborates on a FE CFD model (Gerogiorgis and Ydstie, 2003) developed for a candidate carbothermic aluminium reactor (Johansen and Aune, 2002), aimed at industrial implementation of carbothermic Al production. Carbothermic reduction is an alternative to the conventional Hall-Héroult electrolysis process and is characterized by cost and environmental advantages as well as by a challenging complexity. Process technology encompasses a wide spectrum of phenomena (convection, diffusion, reaction, evaporation, electric field) that occur simultaneously in a multiphase configuration, the geometry of which is an open design problem and remains to be determined without prior experience or even abundance of experimental data. The strong interaction among Joule heating, endothermic reaction, natural Boussinesq convection and turbulent flow phenomena is of paramount importance for understanding reactor performance; conducting CFD simulations is an efficient way to advance with the latter goal, since reliable high-temperature measurements of state variables are remarkably laborious, uncertain and expensive. The quadruple PDE problem (electric charge, heat, momentum and gas volume balances) for the slag flow in the ARP reactor is solved via a commercial CFD software suite (FEMLAB® v. 2.3) to obtain potential, temperature, velocity and gas volume fraction distributions in a two-dimensional domain, representing in detail the complete second stage of the proposed carbothermic reactor. The new challenge is the present paper is to accurately calculate the volume fraction of the gas generated within the molten slag and understand how the proposed geometry affects production, via the instantaneous thermodynamic equilibrium assumption. The main objective of this CFD study is to extract conclusions regarding the reactive slag flow, the extent of space utilization and the existence of dead volumes, and to provide design guidelines. A steady state sensitivity analysis of state variable distributions (namely, potential, temperature, velocity and gas volume fraction) with respect to a key design variable (the imposed voltage profile) reveals the reactor heating potential, the geometry of the Al region and the nontrivial operation, design and optimization problems.

## Introduction: Carbothermic Reduction

The quest for cost-efficient carbothermic reduction technologies is a fascinating chapter of corporate R&D history in its own right, much affected by the energy-intensive nature of Al production and the major energy crises that have plagued it over the decades. A concise historical review of previous major R&D efforts [1] and a thorough presentation of candidate reactors and flowsheets [2] can provide detailed information regarding proposed technologies.

A wide variety of industrial scale process and reactor designs have been proposed in the literature over the years [2]; the complexity has evolved with the advances in understanding complex physics. This study is focusing on a carbothermic aluminium reactor patent of Johansen and Aune assigned to ALCOA and ELKEM [3]; the detailed schematic of the proposed reactor is provided in Figure 1.

## ARP Carbothermic Reactor Engineering

The ARP candidate carbothermic reactor has 4 distinct stages [4]:

1. The *first stage* of the process is a pre-reduction smelting zone. Carbon and aluminium oxide pellets are continuously fed to the submerged arc smelter, melt and react to form a viscous binary molten slag, contained in an inert-atmosphere, oil-cooled reactor. The reaction of aluminium oxide with an excess of carbon to form the $Al_4C_3$-rich slag of the first stage is written as (T > 1900 °C):

$$2Al_2O_{3(s)} + 9C_{(s)} \rightarrow (Al_4C_3+Al_2O_3)_{(slag)} + 6CO_{(g)} \qquad (1)$$

2. The *second stage* is the high-temperature reduction zone: the first-stage molten slag flows slowly into the actual multi-electrode submerged arc reactor, where it is heated to a higher temperature, avoiding local surface superheating caused in open arc reactors. Liquid Al droplets and CO bubbles are rapidly generated at hot spots, while the chemical equilibrium can be assisted by further $Al_4C_3$ injection from the third stage, to avoid carbon depletion. The decomposition of the $Al_4C_3$-rich slag of the first stage to form the Al-rich phase of the second stage is written as (T > 2000 °C):

$$(Al_4C_3 + Al_2O_3)_{(slag)} \rightarrow (6Al + Al_4C_3)_{(metal)} + 3CO_{(g)} \qquad (2)$$

3. The *third stage* consists of a vapor recovery reactor (VRR), where Al and $Al_2O$ vapors react with C to form $Al_4C_3$ [5]. Vaporization occurs as CO vapors sweep the second stage reactor: unless Al species are recovered countercurrent to incoming solid feed, metal loss has a catastrophic impact on process economics, as it is shifting the equilibrium and sharply decreasing yield [6]. This undesirable vaporization effect is reduced by staging and feeding the first and second stage gas streams to the VRR stage. The recovered $Al_4C_3$ (recycle stream) is reinjected into the reactor, minimizing metal vapor emission and maximizing process yield. Energy recovery is possible via heat exchange and cogeneration.

4. The *fourth (final) stage* of the process is the purification zone: liquid aluminium (of lower density than the slag) produced in the second reactor stage flows towards a molten metal separation unit, where entrained solid $Al_4C_3$ particles and dissolved C material can be removed by proprietary technology to recover pure aluminium.

The technical difficulties associated with handling multiphase molten slags at extremely high temperatures (> 2000 °C) [5] and the simultaneous production of Al and $Al_2O$ vapors (inevitable in high-temperature reactor due to localized superheating effects) [6] necessitate a thorough analysis of the temperature distribution [7]. Indeed, in our previous paper, the imposed electrode voltage has been quantitatively proved to govern the location and size of high-temperature regions in the reactor, thus affecting the advance of the endothermic reduction and the volumetric productivity [1]. Therefore, electrode voltage is a crucial reactor design parameter that can also be used very conveniently as a manipulation variable for the efficient operation and control of a carbothermic reactor. The topography of the optimal temperature distribution remains an open problem that entails calculation of concentration profiles.

### Computational Fluid Dynamics Model

The second-stage submerged multielectrode carbothermic reactor does not have symmetry planes and is modeled considering a full two-dimensional domain perpendicular to the major reactor axis at a plane defined by the horizontal electrode circular tips (Figure 1). The resulting two-dimensional computational domain comprises a first-stage molten slag reservoir (melting considered completed), an angled underflow inlet duct feeding the first-stage molten slag, its expansion, and the complete second stage of the ARP reactor, containing six inert graphite electrode tips immersed in the slag.

The full reactor and homogeneous slag assumptions are necessary in order to simplify the complex hierarchy of physical phenomena and study the electric charge, heat, momentum and mass balances. Therefore, the goal here is to solve the steady state PDE problems for the respective variables of the latter balances [potential (V), temperature (T), velocity (U), pressure (P), gas vol. fraction (φ)], and obtain reliable state variable distributions that are elemental in quantitatively understanding and evaluating reactor performance. Thermophysical properties are assumed constant in this study, with two notable exceptions (a) a temperature-dependent density taking into account pure slag density and CO content therein [8, 9] (modeling a pseudohomogeneous coexistence of slag and $CO_{(g)}$), (b) a temperature-dependent electric conductivity that has been also used previously to illustrate the strong coupling between the electric charge balance and the Joule heat generation term [8]. Incompressible flow with buoyancy momentum generation is assumed, and model parameters have already been published [8].

The finite element method is used to formulate the PDE problem on an unstructured triangular domain discretization (Figure 1). The developed finite element model of the reactor has been solved with quadratic finite element basis functions, using a commercial finite element simulation environment (FEMLAB® v. 2.3) [10]. Four FEMLAB® modules have been used for these simulations: (a) "Conductive Media DC", (b) "Convection and Conduction", (c) "K-ε Turbulence Model" and (d) "General form PDE Model". Imposed electrode voltages are crucial, affecting field intensity and current density profiles (hence Joule effect heat production). This is turn is expected to affect the uniformity of heat generation, thus the uniformity of temperature and gas fraction distributions; slag convection is also influenced by the presence of electrodes. This study presents (a) pseudohomogeneous slag CFD results derived without gas generation modeling and (b) two-phase flow CFD results that use a T-independent gas generation model [11].

### CFD Equations and Boundary Conditions

The steady state CFD problem considered in this paper comprises five PDE balances that are solved on a two-dimensional domain. The first part is the steady state electric charge balance:

$$\nabla^2 V = V_{xx} + V_{yy} = 0 \tag{3}$$

The second part is the steady state heat balance:

$$\nabla \cdot (k\nabla T - \rho C_P T\mathbf{U}) + \sigma(\nabla V)^2 - k_0 \exp\left(\frac{-\Delta G}{RT}\right)\Delta H = 0 \tag{4}$$

The third part is the steady state momentum balance:

$$\rho(\mathbf{U}\cdot\nabla\mathbf{U}) - \nabla\cdot\left[\left(\mu + \rho\frac{C_\mu}{\sigma_k}\frac{k^2}{\varepsilon}\right)\cdot\left(\nabla\mathbf{U} + (\nabla\mathbf{U})^T\right)\right] = -\nabla P \tag{5}$$

which also comprises the incompressible continuity PDE:

$$\nabla\cdot\mathbf{U} = 0 \tag{6}$$

complemented with the two standard k-ε model equations:

$$\rho(\mathbf{U}\cdot\nabla k) - \nabla\cdot\left[\left(\mu + \rho\frac{C_\mu}{\sigma_k}\frac{k^2}{\varepsilon}\right)\nabla k\right] = \rho C_\mu \frac{k^2}{\varepsilon}\left(\nabla\mathbf{U} + (\nabla\mathbf{U})^T\right)^2 - \rho\varepsilon \tag{7}$$

$$\rho(\mathbf{U}\cdot\nabla\varepsilon) - \nabla\cdot\left[\left(\mu + \rho\frac{C_\mu}{\sigma_\varepsilon}\frac{k^2}{\varepsilon}\right)\nabla\varepsilon\right] = \rho C_{\varepsilon 1} C_\mu k\left(\nabla\mathbf{U} + (\nabla\mathbf{U})^T\right)^2 - \rho C_{\varepsilon 2}\frac{\varepsilon^2}{k} \tag{8}$$

Finally the two-phase flow is studied using a gas volume balance:

$$\nabla\cdot\left(\mathbf{D}R_b U_s(1-\varphi)\nabla\varphi - U_s\varphi(1-\varphi)\mathbf{e_g} + \varphi\mathbf{U}\right) = 0 \tag{9}$$

The imposed voltages on all electrode tips ($V_i$ , i = 1-6) are set, zero voltage is used on long horizontal sides to approximate the potential in the third lateral dimension, and zero gradient ($\nabla V = 0$) is used on all other wall sides (solidified slag acts as an insulator). Inlet slag (2173 K) and wall (473 K) temperatures are also set, and ideal heat insulation ($\nabla T = 0$) is assumed at all electrode tips. An inlet vertical slag velocity is assumed ($U_0 = 0.01$ m.s$^{-1}$), with either (a) logarithmic wall functions if considering turbulence [12] or (b) a no-slip boundary condition used on reactor walls and tips when explicitly modeling $CO_{(g)}$ generation via Equation (9) [11]. A slip boundary condition is used for the slag free surface and zero pressure has been assumed at the reactor outlet (right end). Elimination of Lorentz (field) and Boussinesq (buoyancy) forces from (5) is based on the use of high-frequency AC electrodes and the negligible heat expansion coefficient of the slag, respectively. Two different stepwise constant voltage profiles are considered.

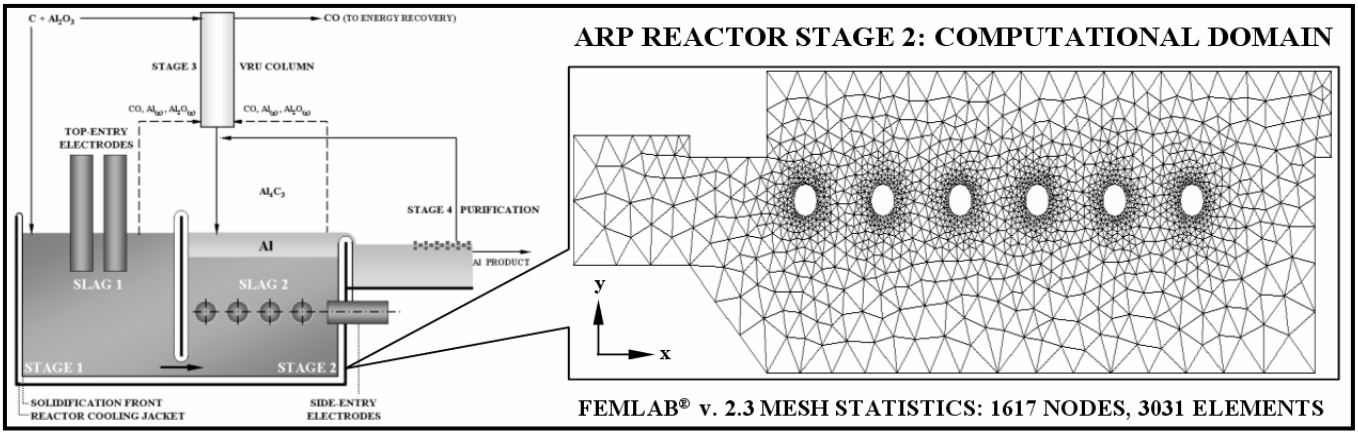


Figure 1: Schematic of the proposed ARP carbothermic aluminium reactor and the corresponding two-dimensional computational domain.

**CFD Simulation Results: Case 1** $V_1 = V_2 = V_3 = V_4 = V_5 = V_6 = 50$ V

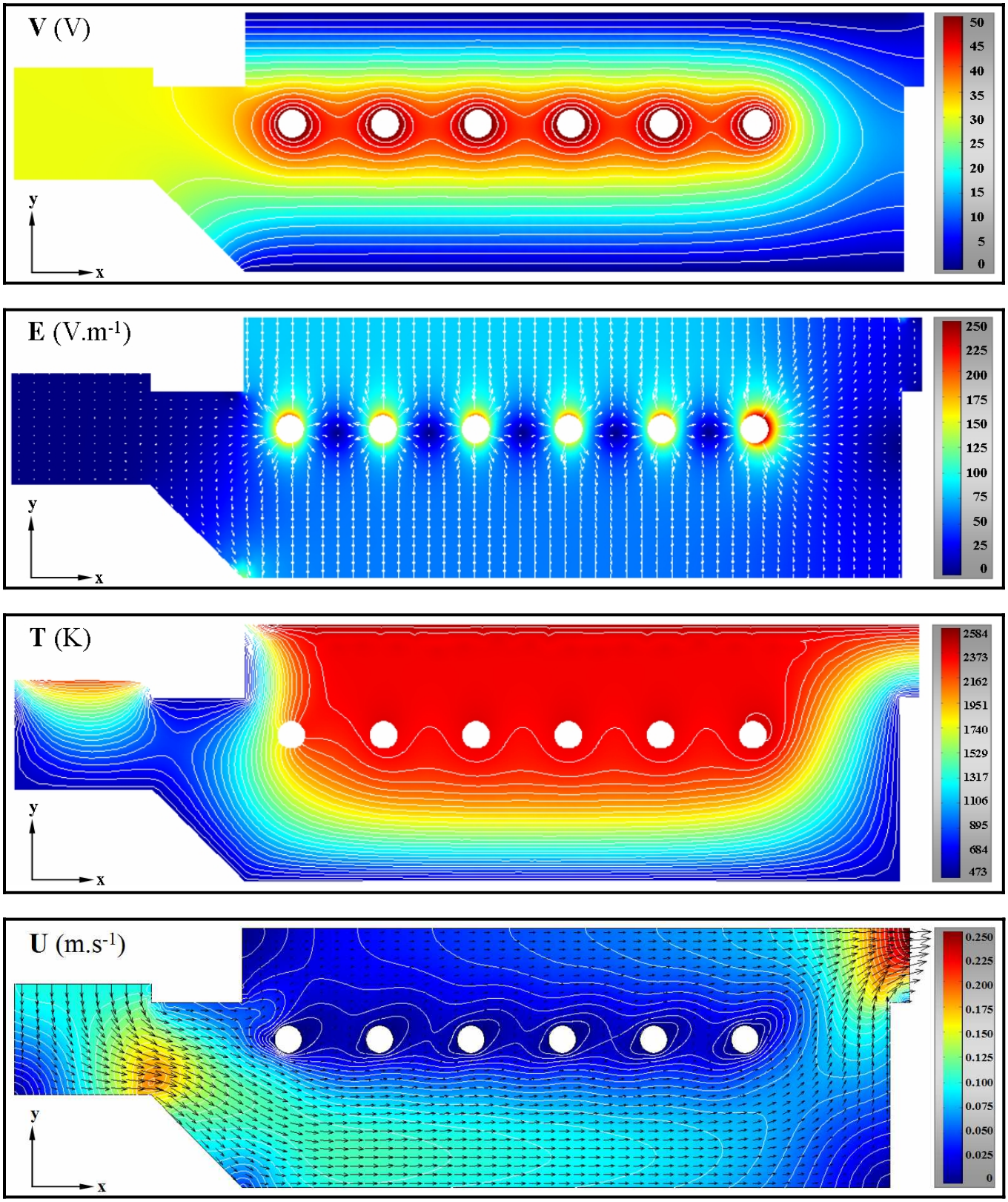


Figure 2: Potential (V), field intensity (E), temperature (T) and slag velocity (U) distributions – U is without gas generation (first case).

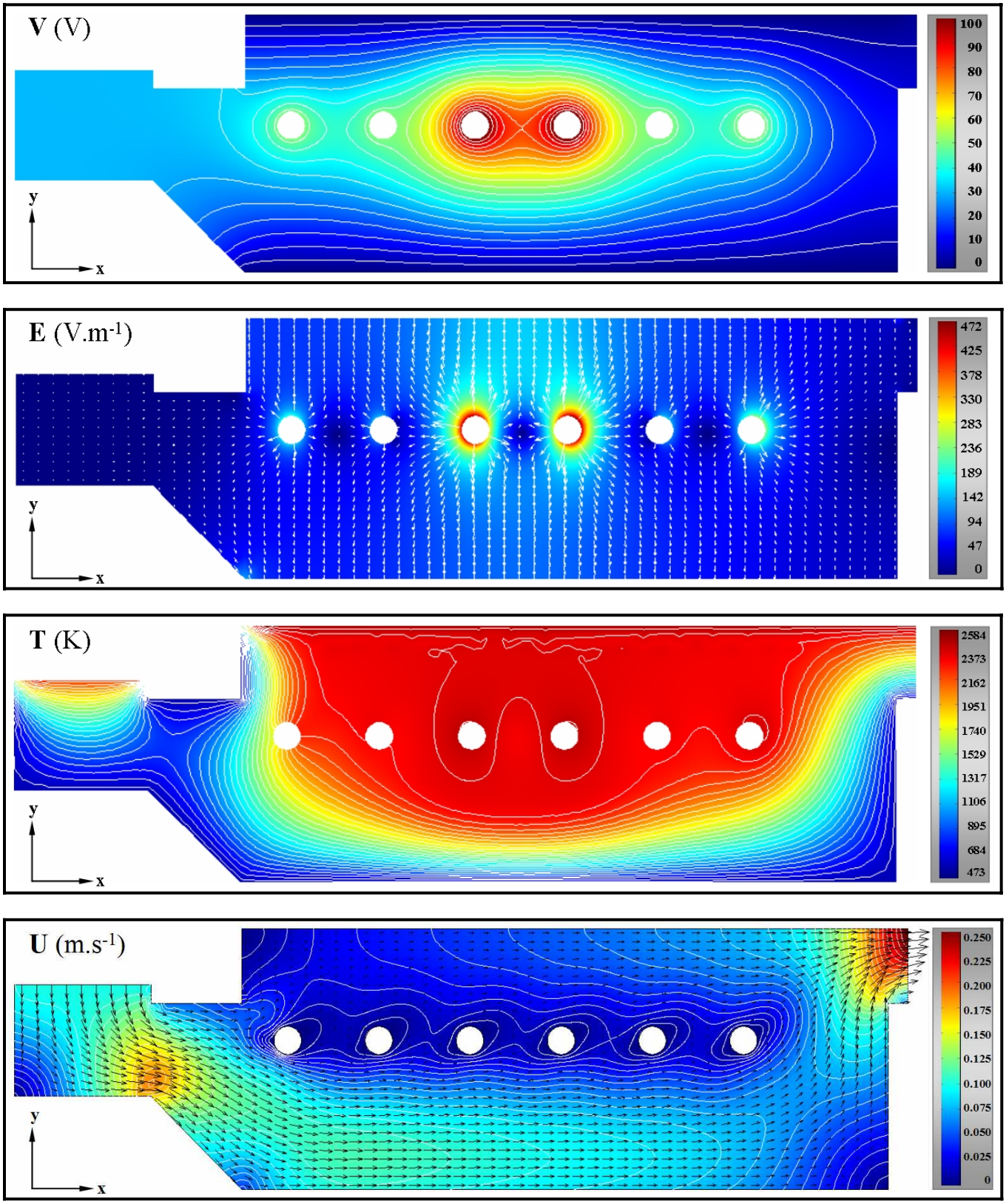


Figure 3: Potential (V), field intensity (E), temperature (T) and slag velocity (U) distributions – U is without gas generation (second case).

**CFD Simulation Results: Case 1 and Case 2 with Explicit Gas Generation Modeling**

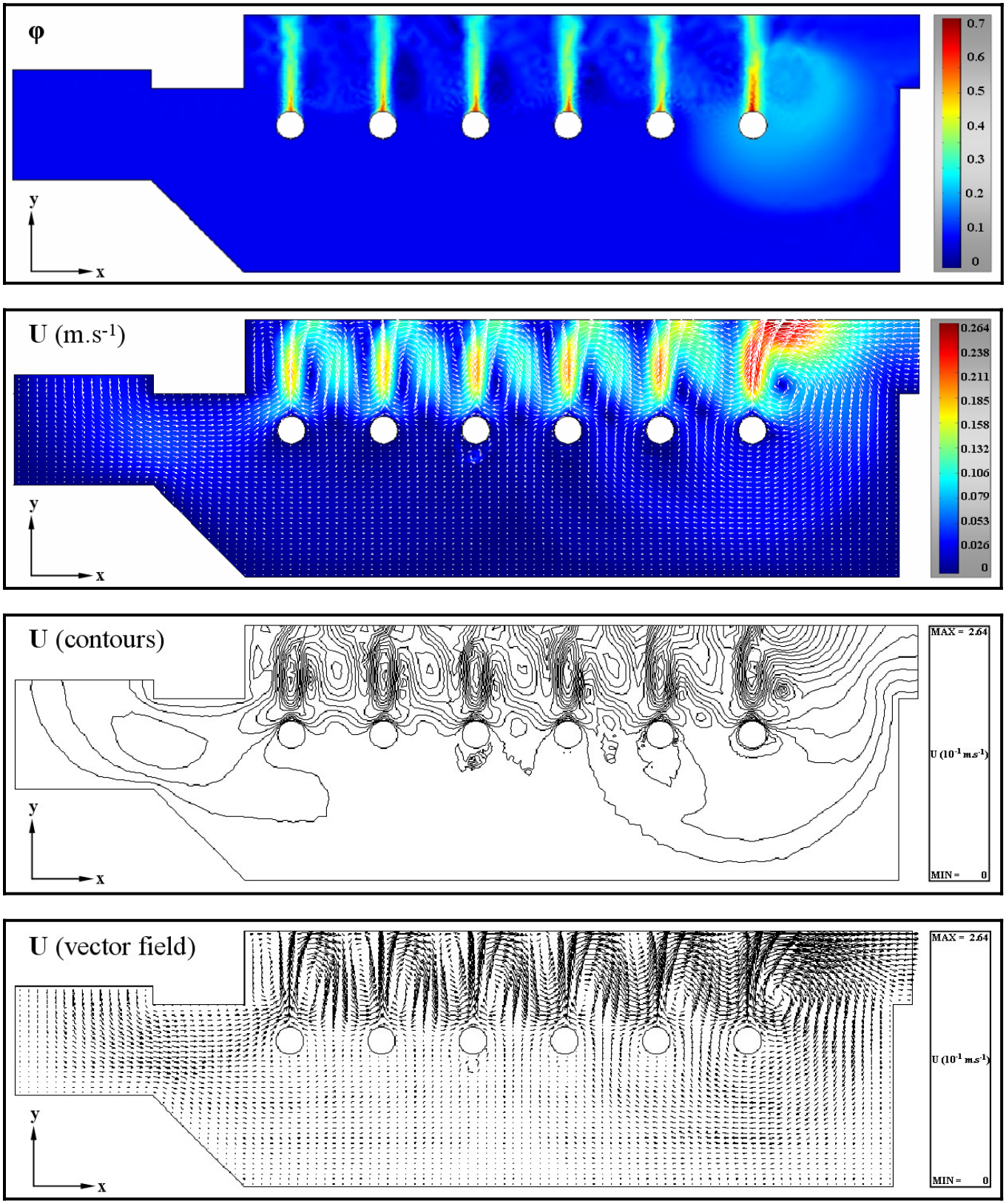


Figure 4: Gas volume fraction (φ), slag velocity (U) distribution, contours and vector field – U is with explicit gas generation modeling.

## Conclusions and Future Goals

The present integrated multiphysics CFD modeling study analyzes a candidate design for a carbothermic aluminium reactor via a sensitivity analysis performed for two possible voltage profiles. Potential, temperature, velocity and gas fraction distributions obtained by simultaneous solution of electric charge, heat, mass, momentum and volume balances reveal several remarkable trends. Because voltage is identified as a convenient design variable [1], the goal is to study and understand its effect on reactor operation by a sensitivity analysis performed for 2 different voltage profiles.

The use of quadratic finite element basis functions has been particularly successful for the purpose of all present simulations: the standard nonlinear solver that is provided in FEMLAB® 2.3 has been used effectively to conduct the computational analysis. The CPU time required for convergence below tolerance ($10^{-10}$) when solving the quadruple PDE problem for specific voltages ($V_i$) is about 30 min. (the corresponding grid has 3031 triangles). Solutions are obtained using reasonable computational resources (a Pentium III / 1.2 GHz with 512 MB of RAM has been used). Finer discretizations will have to be used for enhanced accuracy.

Electric potential (V) distributions are presented in Figures 2, 3 for the 2 different electrode voltage profiles considered ($V_i$): they are symmetric about the horizontal reactor axis (electrode line) and indicate certain polarization on the left molten slag reservoir, consistent with the presence of the first-stage electrodes therein. There are remarkable differences between the two cases, related to the size and the uniformity of the high-V area in the reactor core.

Field intensity (E) distributions are depicted in Figures 2, 3 and indicate a clear localization of electric activity (Joule heating) close to the periphery of electrodes, where E maxima are found. Local minima are also evident on the line in between electrodes. Joule heat production is greatly affected by these sharp E extrema, as proportional to the square of the field intensity [ $Q_H = \sigma(\nabla V)^2$ ].

Temperature (T) distributions are presented in Figures 2, 3 and are characterized by an extended, high-temperature reactor core zone and a cooled slag containment zone formed against reactor walls. Although temperature plots are clearly different for the two profiles, the maximum temperature reached (2584 K) is identical. The CO generation rate is considered independent of temperature in this study; thus, T profiles are not affected by gas production.

Slag velocity field (U) distributions are depicted in Figures 2, 3 (for the pseudohomogeneous slag case without gas generation), and in Figure 4 (for the two-phase flow case with gas generation). A rapid turbulent flow zone at the underflow contraction and substantial circulation at the reactor bottom (Figures 2,3) indicate that convection domination therein decreases temperature notably. Turbulent kinetic energy dissipation diminishes U gradients there. The generation and presence of $CO_{(g)}$ at and near all six electrodes affects the U profile significantly compared to previous work [13], confirming the need for explicit two-phase flow CFD simulations.

The gas volume fraction ($\varphi$) distribution presented in Figure 4 indicates that $CO_{(g)}$ generation is significant and has a major effect on the slag flow (our assumption that gas generation only occurs on electrode surfaces is justified by the temperature distribution). Recirculation zones are apparent in between electrode pairs, and they seem to affect the flow pattern only above the electrode line. The detailed calculation of species concentrations is our next goal.

## Acknowledgements

The authors acknowledge helpful discussions with Dr. D. Roha of ALCOA as well as the financial support provided by ALCOA Inc. This study is part of a project co-funded by the U.S. Department of Energy (jointly undertaken by ALCOA Inc., ELKEM ASA Research and Carnegie Mellon University) for the investigation of the technical feasibility of carbothermic aluminium production. The first author gratefully acknowledges a Fulbright fellowship awarded by the U.S. Institute of International Education (IIE) as well as a doctoral fellowship awarded by the Onassis Foundation.

## References

1. D.I. Gerogiorgis, B.E. Ydstie, "A Finite Element CFD Sensitivity Analysis for the Conceptual Design of a Carbothermic Aluminium Reactor," *Light Metals 2003*, ed. P. Crepeau (Warrendale, PA: TMS, 2003), 407-414.

2. K. Motzfeldt et al., *Carbothermal Production of Aluminium – Chemistry and Technology* (Dusseldorf: Alum. Verlag, 1989).

3. K. Johansen and J. Aune, U.S. Patent 6,440,193 (2002).

4. K. Johansen et al., "Carbothermic Aluminum", in: *Proceedings of the Sixth International Conference on Molten Slags, Fluxes and Salts* (paper #192); Stockholm, Sweden (CD edition).

5. K. Johansen et al., "Aluminum Carbothermic Technology: ALCOA-ELKEM Advanced Reactor Process," *Light Metals 2003*, ed. P. Crepeau (Warrendale, PA: TMS, 2003), 401-406.

6. M. Bruno, "Aluminum Carbothermic Technology: Comparison to Hall-Héroult Process," *Light Metals 2003*, ed. P. Crepeau (Warrendale, PA: TMS, 2003), 395-400.

7. D.I. Gerogiorgis, B.E. Ydstie, M. Bruno, K. Johansen, "Process Systems Tools for Design and Optimization of Carbothermic Reduction Processes," *Aluminum 2003*, ed. S. K. Das (Warrendale, PA: TMS, 2003), 289-298.

8. D.I. Gerogiorgis, B.E. Ydstie, S.S. Seetharaman, "A Steady State Electrothermic Simulation Analysis of a Carbothermic Reduction Reactor for the Production of Aluminium," *Comput. Modeling of Materials, Minerals and Metals Processing*, ed. M. Cross et al. (Warrendale, PA: TMS, 2002), 273-282.

9. B. Glorieux et al., "Density of Superheated and Undercooled Liquid Alumina by a Contactless Method," *Int. J. Thermophys.*, 20 (4) (1999), 1085-1094.

10. FEMLAB® 2.3 Ref. Manual, (Stockholm: COMSOL, 2002).

11. R. Wetind, "Two-Phase Flow in Gas-Evolving Electrochemical Applications," Ph.D. Thesis (Stockholm: KTH, 2001).

12. T.J. Chung, *Computational Fluid Dynamics* (Cambridge, UK: Cambridge University Press, 2002).

13. D.I. Gerogiorgis, B.E. Ydstie, "Flow Modeling for Design of Carbothermic Aluminium Reactors," *Proceedings of the Third International Conference on CFD in the Minerals and Process Industries*, ed. M. P. Schwarz (Melbourne, Australia: CSIRO, 2003), in press.